

Topological spin Hall and spin Nernst effects in a bilayer graphene

A. Dyrda¹, J. Barnaś^{1,2}

¹*Department of Physics, Adam Mickiewicz University, ul. Umultowska 85, 61-614 Poznań*

²*Institute of Molecular Physics, Polish Academy of Sciences,
ul. M. Smoluchowskiego 17, 60-179 Poznań, Poland*

(Dated: June 4, 2018)

We consider intrinsic contributions to the spin Hall and spin Nernst effects in a bilayer graphene. The relevant electronic spectrum is obtained from the tight binding Hamiltonian, which also includes the intrinsic spin-orbit interaction. The corresponding spin Hall and spin Nernst conductivities are compared with those obtained from effective Hamiltonians appropriate for states in the vicinity of the Fermi level of a neutral bilayer graphene. Both conductivities are determined within the linear response theory and Green function formalism. The influence of an external voltage between the two atomic sheets is also included. We found transition from the topological spin Hall insulator phase at low voltages to conventional insulator phase at larger voltages.

PACS numbers: 73.43.-f, 72.25.Hg, 73.61.Wp

I. INTRODUCTION

Four decades ago Dyakonov and Perel showed that a system with strong spin-orbit interaction should reveal transverse spin current and spin accumulation in the presence of external longitudinal electric field^{1,2} – even if the system is nonmagnetic. This effect, known now as the spin Hall effect (SHE)³, was studied extensively in the last few years^{3–9}, and is still of current interest – mainly because it offers a new possibility of spin manipulation with electric field only. The possibility of pure electrical manipulation of spin degrees of freedom is interesting not only from fundamental reasons, but also from the point of view of possible applications in future spintronics devices and information processing technologies^{10–13}.

The crucial interaction responsible for SHE, i.e. the spin-orbit coupling, may be either of intrinsic (internal) or extrinsic origin. The corresponding extrinsic SHE is associated with mechanisms of spin-orbit scattering on impurities and other defects (skew scattering and/or side jump), while the intrinsic SHE is a consequence of a nontrivial trajectory of charge carriers in the momentum space due to the spin-orbit contribution of a perfect crystal lattice to the corresponding band structure. The intrinsic SHE may be described in terms of the Berry phase formalism^{14,15} and therefore it is also referred to as the topological SHE.

It is well known that various spin effects, like for instance spin current and spin accumulation, may be generated not only by external electric field, but also due to a temperature gradient. Indeed, there is a great interest currently in spin related thermoelectric effects. One of such phenomena is the spin Seebeck effect, where longitudinal spin current and spin voltage are generated by a temperature gradient¹⁶. Of particular interest, however, are spin thermoelectric effects in systems with spin-orbit interaction, where a temperature gradient gives rise to transverse spin accumulation and/or spin currents. Thus, the temperature gradient in such systems may lead to anomalous (in case of ferromagnetic systems) and spin

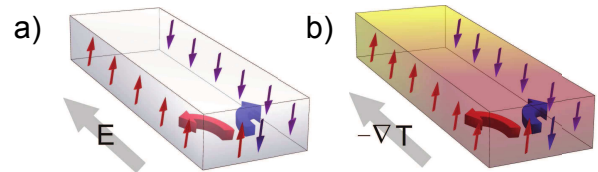


FIG. 1. (color on-line) Schematic presentation of transverse spin accumulation induced by (a) electric field (spin Hall effect) and (b) temperature gradient (spin Nernst effect).

Nernst effects^{17–19}, which correspond to the anomalous and spin Hall effects induced by longitudinal electric field. Similarity of the spin Hall and spin Nernst effects in nonmagnetic systems with spin-orbit interaction is presented in Fig.1, which clearly shows that the SHE is generated by external electric field, while the spin Nernst effect (SNE) is a similar effect generated by a temperature gradient instead of electric field (gradient of electrostatic potential).

In this paper we consider the topological contribution to the spin Hall and spin Nernst effects in a bilayer graphene. Graphene is a two-dimensional crystal of carbon atoms. A monolayer graphene in a free standing form was obtained few years ago and owing to its unusual and peculiar properties quickly became one of the most extensively studied materials^{20–22}. After the pioneering paper by Kane and Mele²³, spin Hall effect in a monolayer graphene was studied in many papers and in various physical situations. Recently, bilayer graphene is extensively studied as a more appropriate for applications than a single-layer one. Moreover, it has been shown that spin-orbit coupling in a bilayer can be enhanced in comparison to that in a single-layer graphene²⁴. This motivated us to consider topological contributions to the SHE and SNE in a bilayer graphene.

Both SHE and SNE in (nonmagnetic) graphene are generated by spin-orbit interaction. In general, one can distinguish two different forms of the spin-orbit interac-

tion having the crystal lattice periodicity and contributing to the relevant band structure – internal and Rashba spin-orbit interactions. The latter interaction is due to a substrate and can be controlled by an external gate voltage. In this paper we consider the contributions to SHE and SNE due to the intrinsic spin-orbit interaction only. It is known that this interaction opens an energy gap at the Dirac points. It was also shown that the energy gap can be tuned externally by applying a voltage bias between the layers^{25,26}. The gate voltage dependence of the spin Hall conductivity, leading to phase transition between the spin Hall insulator and classical insulator will also be considered in this paper.

The description of transport properties of graphene is usually based on some effective Hamiltonian, which properly describes electronic spectrum near the Fermi level of a neutral system. However, it is well known that the topological contribution to the spin Hall effect includes contributions from electronic states far below the Fermi level, and therefore a more accurate electronic spectrum is required to describe the effect properly. Accordingly, in this paper we calculate the spin Hall and spin Nernst conductivities from a more realistic electronic spectrum based on a tight binding Hamiltonian, and compare them with the corresponding conductivities obtained on the basis of effective Hamiltonians. The results presented in this paper reveal, however, a very good agreement between the conductivities derived from the effective and tight binding Hamiltonians.

The paper is organized as follows. In section 2 we describe briefly the electronic states of a bilayer graphene within the tight binding Hamiltonian and also in terms of an effective Hamiltonian, which is sufficient for states in the vicinity of the Fermi level of a neutral graphene. In both cases the intrinsic spin-orbit interaction and the effect of a normal bias voltage are taken into account. In section 3 we calculate the spin Hall and spin Nernst conductivities for the tight binding Hamiltonian and compare them with those obtained from the effective Hamiltonian. In the latter case we derive analytical formulas for the spin Hall and spin Nernst conductivities. We also discuss the role of normal bias (in the framework of the effective model). Description based on a reduced low-energy effective Hamiltonian is presented in section 4. Summary and final conclusions are given in section 5.

II. ELECTRONIC SPECTRUM OF THE BILAYER GRAPHENE

A single-layer graphene is a monolayer of carbon atoms arranged in a two-dimensional honeycomb lattice which can be also considered as being composed of two nonequivalent triangular sublattices. In the absence of spin-orbit interaction the Fermi surface of a neutral single-layer graphene consists of two nonequivalent K and K' points of the Brillouin zone, at which the valence and conduction bands touch each other. The cor-

responding electronic spectrum can be described by a tight binding Hamiltonian with nearest and next-nearest neighbor hopping terms. The low energy electron states near the points K and K' can be well approximated by a conical energy spectrum (linear dispersion relations). As a result, charge carriers in the vicinity of the points K and K' are described effectively by the relativistic Dirac equation.^{20,21} Intrinsic spin-orbit interaction opens then an energy gap at the Dirac points.²³ The tight binding and effective Hamiltonians for a bilayer graphene are more complex, as described below.

A. Tight binding model

The bilayer graphene in the Bernal stacking (see *eg* [22]) is described by the following tight binding Hamiltonian:

$$\mathcal{H} = \int d^2\mathbf{k} \psi(\mathbf{k})^\dagger \begin{pmatrix} H & \Gamma \\ \Gamma^\dagger & H \end{pmatrix} \psi(\mathbf{k}), \quad (1)$$

where

$$H = \begin{pmatrix} h_{so}S_z + VS_0 & h_0S_0 \\ h_0^*S_0 & -h_{so}S_z - VS_0 \end{pmatrix}, \quad (2)$$

$$\Gamma = \begin{pmatrix} 0 & \gamma_1 S_0 \\ 0 & 0 \end{pmatrix}. \quad (3)$$

The matrix elements h_0 and h_{so} are defined as follows: $h_0 = -t[e^{i2bk_y/3} + 2 \cos(\frac{1}{2}ak_x) e^{-ibk_y/3}]$ and $h_{so} = -2t'[\sin(ak_x) - 2 \sin(ak_x/2) \cos(bk_y)]$, where t is the hopping integral between the nearest neighbors in the atomic sheets, t' is the next-nearest neighbor spin-orbit hopping amplitude, while $b = a\sqrt{3}/2$ with a being the lattice parameter. Furthermore, V is the voltage between the two atomic sheets of the bilayer (measured in energy units), S_α denote the unit ($\alpha = 0$) and Pauli ($\alpha = x, y, z$) matrices in the spin space, while γ_1 describes coupling between the two atomic layers.

The corresponding energy eigenvalues for $V = 0$ have then the following form:

$$E_{1,2} = \mp \left[h_{so}^2 + \frac{1}{2} \left(\gamma_1^2 + 2h_0^2 - \gamma_1 \sqrt{\gamma_1^2 + 4h_0^2} \right) \right]^{1/2} \quad (4)$$

$$E_{3,4} = \mp \left[h_{so}^2 + \frac{1}{2} \left(\gamma_1^2 + 2h_0^2 + \gamma_1 \sqrt{\gamma_1^2 + 4h_0^2} \right) \right]^{1/2} \quad (5)$$

This spectrum is shown in Fig.2(a). States near the point K are shown by the solid lines in parts (b) and (c). The part (c) reveals a small energy gap created at the Dirac points by the spin-orbit interaction.

When $V \neq 0$, the inversion symmetry is broken (layers are no longer equivalent) and the degeneracy is lifted. The corresponding eigenvalues acquire then the form

$$E_{1,2} = \mp \left[h_0^2 + h_{so}^2 + V^2 + \frac{\gamma_1^2}{2} - \frac{1}{2} [(\gamma_1^2 - 4Vh_{so})^2 + 4(\gamma_1^2 + 4V^2)h_0^2]^{1/2} \right]^{1/2}, \quad (6)$$

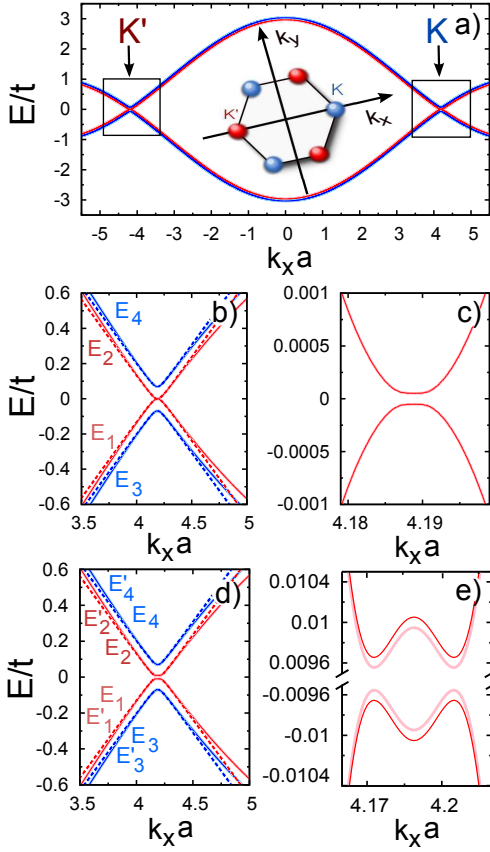


FIG. 2. Electronic spectrum of the bilayer graphene in the tight binding model for $k_y = 0$, $t = 2.9$ eV, $t'/t = 10^{-5}$, $\gamma_1/t = 0.069$, and $V = 0$ (a). The tight binding energy spectrum in the vicinity of the K point (solid lines) and the corresponding energy spectrum obtained from the effective model (dotted lines) are compared in (b) for $V = 0$ and in (d) for $V/t = 0.01$. Parameters of the effective model, corresponding to the tight binding one, are: $\Delta_{so} = 0.15$ meV and $v = 3.516 \times 10^{-10}$ eVm. The electron states very close to the energy gap are shown in (c) for $V = 0$ and in (e) for $V/t = 0.01$ (here the results from the tight binding and effective Hamiltonians overlap).

$$E_{1',2'} = \mp \left[h_0^2 + h_{so}^2 + V^2 + \frac{\gamma_1^2}{2} - \frac{1}{2} [(\gamma_1^2 + 4Vh_{so})^2 + 4(\gamma_1^2 + 4V^2)h_0^2]^{1/2} \right]^{1/2} \quad (7)$$

$$E_{3,4} = \mp \left[h_0^2 + h_{so}^2 + V^2 + \frac{\gamma_1^2}{2} + \frac{1}{2} [(\gamma_1^2 - 4Vh_{so})^2 + 4(\gamma_1^2 + 4V^2)h_0^2]^{1/2} \right]^{1/2}, \quad (8)$$

$$E_{3',4'} = \mp \left[h_0^2 + h_{so}^2 + V^2 + \frac{\gamma_1^2}{2} + \frac{1}{2} [(\gamma_1^2 + 4Vh_{so})^2 + 4(\gamma_1^2 + 4V^2)h_0^2]^{1/2} \right]^{1/2} \quad (9)$$

The corresponding spectrum for the assumed value of $V/t = 0.01$ is indistinguishable from the spectrum shown in Fig.2(a) for $V = 0$. The differences can be seen on a smaller energy scale, as in the parts (d) and (e) of Fig.2. When comparing Figs 2(b) and 2(d), one can notice a larger energy gap for $V/t = 0.01$. This is more clearly seen when comparing the parts (c) and (e). First, for the assumed value of V the gap is wider than for $V = 0$. Second, the top and bottom band edges become split and shifted away from the Dirac points. As will be described later, the applied voltage between the atomic sheets first closes the gap and then opens a new one with the width increasing with V .

B. Effective Hamiltonian

When only electronic states near the Fermi level (near the Dirac points) of a neutral graphene are relevant, one can make use of some effective Hamiltonians to describe the corresponding electronic spectrum. Such a Hamiltonian can be derived using the $\mathbf{k} \cdot \mathbf{p}$ approximation. As a result, the effective Hamiltonian for states near the K point of the bilayer graphene takes the form^{27,28}:

$$H_K = \mathcal{T}_0 \otimes H_K^s - \frac{\gamma_1}{2} (\mathcal{T}_x \otimes \sigma_x \otimes S_0 - \mathcal{T}_y \otimes \sigma_y \otimes S_0), \quad (10)$$

where

$$H_K^s = v(k_x \sigma_x + k_y \sigma_y) \otimes S_0 + \Delta_{so} \sigma_z \otimes S_z + V \sigma_0 \otimes S_0. \quad (11)$$

The first term on the right side corresponds to two decoupled atomic monolayers, each of them being described by the Kane Hamiltonian for a single layer graphene, H_K^s . In turn, the second term describes coupling between the monolayers, with \mathcal{T}_α denoting respectively the unit matrix ($\alpha = 0$) and Pauli ($\alpha = x, y, z$) matrices associated with the layer degree of freedom. In turn, σ_α ($\alpha = 0, x, y, z$) are the unit ($\alpha = 0$) and Pauli ($\alpha = x, y, z$) matrices in the pseudo-spin (sublattice) space. Relations between the parameters of the tight binding and Kane models are: $v = \sqrt{3}ta/2 = \hbar v_F$ (v_F is the carrier velocity at the Fermi level) and $\Delta_{so} = 3\sqrt{3}t'$.

The eigenvalues of Hamiltonian (10) for $V = 0$ take the form

$$E_{1,2} = \mp \left[k^2 v^2 + \frac{\gamma_1^2}{2} + \Delta_{so}^2 - \frac{\gamma_1}{2} \sqrt{4k^2 v^2 + \gamma_1^2} \right]^{1/2} \quad (12)$$

and

$$E_{3,4} = \mp \left[k^2 v^2 + \frac{\gamma_1^2}{2} + \Delta_{so}^2 + \frac{\gamma_1}{2} \sqrt{4k^2 v^2 + \gamma_1^2} \right]^{1/2}. \quad (13)$$

Electronic spectrum near the point K, described by the above formula, is shown in Fig.2(b,c), where it is compared with the spectrum obtained from the full tight binding Hamiltonian. Close to the K point (gap), spectra from both models coincide very well.

When $V \neq 0$, one finds

$$E_{1,2} = \mp \left[v^2 k^2 + \Delta_{so}^2 + V^2 + \frac{\gamma_1^2}{2} - \frac{1}{2} [(\gamma_1^2 - 4V\Delta_{so})^2 + 4v^2 k^2 (\gamma_1^2 + 4V^2)]^{1/2} \right]^{1/2} \quad (14)$$

$$E_{1',2'} = \mp \left[v^2 k^2 + \Delta_{so}^2 + V^2 + \frac{\gamma_1^2}{2} - \frac{1}{2} [(\gamma_1^2 + 4V\Delta_{so})^2 + 4v^2 k^2 (\gamma_1^2 + 4V^2)]^{1/2} \right]^{1/2} \quad (15)$$

$$E_{3,4} = \mp \left[v^2 k^2 + \Delta_{so}^2 + V^2 + \frac{\gamma_1^2}{2} + \frac{1}{2} [(\gamma_1^2 - 4V\Delta_{so})^2 + 4v^2 k^2 (\gamma_1^2 + 4V^2)]^{1/2} \right]^{1/2} \quad (16)$$

$$E_{3',4'} = \mp \left[v^2 k^2 + \Delta_{so}^2 + V^2 + \frac{\gamma_1^2}{2} + \frac{1}{2} [(\gamma_1^2 + 4V\Delta_{so})^2 + 4v^2 k^2 (\gamma_1^2 + 4V^2)]^{1/2} \right]^{1/2} \quad (17)$$

The above spectrum is shown in Fig.3(d,e), where it is compared with the corresponding spectrum obtained in the tight binding model. As before, spectra from tight-binding and effective models coincide near the K point. Note, the band splitting due to V is well resolved only in part (e).

Separation of the bands E_3 and E_4 in the effective model described above, as well as in the tight binding model, is much larger than the separation of the bands E_1 and E_2 , see Fig.2. Therefore, when the electronic states close to the band edges are relevant and sufficient to describe transport properties (eg. when the Fermi level is in the gap), one may restrict considerations to the bands E_1 and E_2 . This leads to a further simplification of the effective Hamiltonian, as described in more details in section 4.

III. SPIN HALL AND SPIN NERNST EFFECTS

Spin Hall and spin Nernst effects correspond to transversal spin currents induced by electric field and temperature gradient, respectively. By analogy to the usual Hall and Nernst effects one may write the density of spin current due to electric field \mathbf{E} and temperature gradient ∇T as

$$J_i^{s_n} = \sum_j [\sigma_{ij}^{s_n} E_j + \alpha_{ij}^{s_n} (-\partial_j T)] \quad (18)$$

where $\sigma_{ij}^{s_n}$ (for $i, j = x, y$) is the spin Hall conductivity with $s_n = (\hbar/2)\sigma_n$ being the n -th component ($n = x, y, z$) of electron spin, while $\alpha_{ij}^{s_n}$ denotes the thermoelectric spin Nernst conductivity. The two conductivities are not independent and obey some general relations. Our objective is to find first the zero-temperature spin Hall conductivity, and then to calculate the low-temperature thermoelectric spin Nernst conductivity from these relations, as described below.

The quantum-mechanical operator of spin current density may be defined as

$$\mathbf{J}^{s_n} = \frac{1}{2} [\mathbf{v}, s_n]_+, \quad (19)$$

where $[A, B]_+ = AB + BA$ denotes the anticommutator of any two operators A and B , while $v_i = (1/\hbar)(\partial H/\partial k_i)$ is the velocity operator ($i = x, y$). The latter operator can be easily found from the corresponding Hamiltonian [Eqs (1) and (10)]. In the linear response theory, the frequency-dependent spin Hall conductivity is then given by the formula²⁹,

$$\sigma_{xy}^{s_z}(\omega) = \frac{e\hbar}{2\omega} \text{Tr} \int \frac{d\varepsilon}{2\pi} \frac{d^2\mathbf{k}}{(2\pi)^2} [v_x, s_z]_+ G_{\mathbf{k}}(\varepsilon + \omega) v_y G_{\mathbf{k}}(\varepsilon), \quad (20)$$

where $G_{\mathbf{k}}(\varepsilon)$ is the Green function corresponding to the appropriate Hamiltonian of the system. When we restrict considerations to the topological contribution to the spin Hall current in the d.c. limit, this formula gives exactly the same result as that based on the Berry phase calculations¹⁴ in momentum space.

It has been shown that the Berry phase leads to an additional term in the general expression for the orbital magnetization³⁰. This correction gives rise to some contributions to the charge and spin currents^{17,31}, and also allows to write the relationship between intrinsic spin Nernst conductivity and intrinsic zero-temperature spin Hall conductivity, which in the low-temperature regime takes the form³¹

$$\alpha_{xy}^{s_z} = \frac{\pi^2 k_B^2}{3e} T \left. \frac{d\sigma_{xy}^{s_z}}{d\varepsilon} \right|_{\varepsilon=\mu}, \quad (21)$$

where T stands for temperature and k_B denotes the Boltzman constant. The latter equation is the spin analog of the Mott relation for charge transport, and will be used to calculate the low-temperature spin Nernst conductivity from the zero-temperature spin Hall conductivity. The derivative in Eq.(21) is taken at the Fermi level μ . The latter can be tuned by an external gate voltage.

Thus, we need to calculate the spin Hall conductivity first. The relevant derivation depends on the model applied to describe the corresponding electronic spectrum. Below we present derivation of the conductivity for the effective Hamiltonian, where analytical results are available. These results will be compared with those obtained numerically for the tight binding model.

A. The limit of $V = 0$

Assume first the limit of $V = 0$. To find the spin Hall conductivity we start from Eq.(20) and write it in the form

$$\begin{aligned} \sigma_{xy}^{s_z}(\omega) &= \frac{e}{2\omega} \int \frac{d\varepsilon}{2\pi} \int \frac{d^2\mathbf{k}}{(2\pi)^2} D(\varepsilon + \omega, \varepsilon) \\ &\times \prod_{n=1}^4 [\varepsilon - E_n + \omega + \mu + i\delta \text{sign}(\varepsilon)]^{-2} \\ &\times \prod_{m=1}^4 [\varepsilon - E_m + \mu + i\delta \text{sign}(\varepsilon)]^{-2}. \end{aligned} \quad (22)$$

Here, $D(\varepsilon + \omega, \varepsilon)$ is defined as

$$D(\varepsilon + \omega, \varepsilon) = \text{Tr}\{[v_x, s_z]_+ g_{\mathbf{k}}(\varepsilon + \omega) v_y g_{\mathbf{k}}(\varepsilon)\}, \quad (23)$$

where $g_{\mathbf{k}}(\varepsilon)$ denotes the nominator of the corresponding Green function $G_{\mathbf{k}}(\varepsilon)$. Taking the first two terms of the expansion of $D(\varepsilon + \omega, \varepsilon)$ with respect to ω , one finds

$$D(\varepsilon + \omega, \varepsilon) \simeq i\omega\chi(\varepsilon), \quad (24)$$

with

$$\begin{aligned} \chi(\varepsilon) &= 8v^2\Delta_{so} \{v^2k^2 [v^2k^2 + 2(\Delta^2 - (\varepsilon + \mu)^2)] \\ &+ (\Delta_{so}^2 - (\varepsilon + \mu)^2)(\gamma_1^2 + \Delta_{so}^2 - (\varepsilon + \mu)^2)\}^2 \\ &\times \{(\Delta_{so}^2 - (\varepsilon + \mu)^2)(\gamma_1^2 + \Delta_{so}^2 - (\varepsilon + \mu)^2) \\ &+ v^2k^2 [v^2k^2 + 2(\gamma_1^2 + \Delta_{so}^2 - (\varepsilon + \mu)^2)]\}. \end{aligned} \quad (25)$$

Thus, in the limit of $\omega \rightarrow 0$ one finds the following expression for the spin Hall conductivity

$$\sigma_{xy}^{s_z} = i\frac{e}{2} \int \frac{d\varepsilon}{2\pi} \int \frac{d^2\mathbf{k}}{(2\pi)^2} \mathcal{F}(\varepsilon), \quad (26)$$

where

$$\mathcal{F}(\varepsilon) = \frac{\chi(\varepsilon)}{\prod_{n=1}^4 [(\varepsilon - E_n + \mu + i\delta \text{sign}(\varepsilon))^4]}. \quad (27)$$

Integrating now over ε one finds

$$\int d\varepsilon \mathcal{F}(\varepsilon) = 2\pi i \sum_n R_n f(E_n), \quad (28)$$

where R_n ($n = 1 - 4$) are the residues associated with the corresponding selfenergies (electron bands), and $f(E)$ is the Fermi distribution function (here for zero temperature). These residues are equal:

$$R_{1,2} = \pm \frac{4\sqrt{2}v^2\Delta_{so} [2v^2k^2(\gamma_1 + \xi) + \gamma_1(\gamma_1^2 - \gamma_1\xi + 2\Delta_{so}^2)]}{\xi^3 (2v^2k^2 + \gamma_1^2 - \gamma_1\xi + 2\Delta_{so}^2)^{3/2}} \quad (29)$$

and

$$R_{3,4} = \pm \frac{8\sqrt{2}v^2\Delta_{so}L}{\xi^3 (2v^2k^2 + \gamma_1^2 + \gamma_1\xi + 2\Delta_{so}^2)^{5/2}} \quad (30)$$

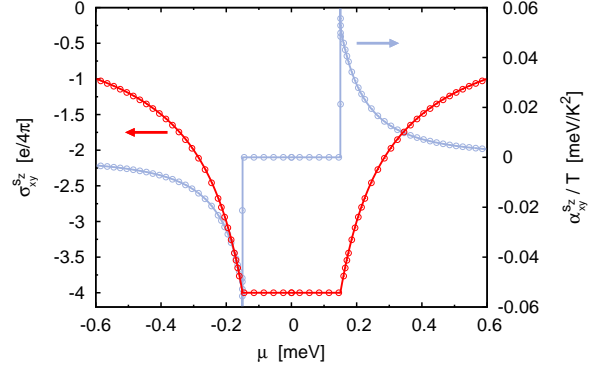


FIG. 3. (color on-line) Spin Hall and spin Nernst conductivities of a bilayer graphene for $V = 0$ and other parameters as in Fig.2. Contributions from both K and K' points are included. The solid lines correspond to the results obtained from the effective Hamiltonian (10), while the dotted ones from the tight binding model.

with

$$\begin{aligned} L &= -v^2k^2(3\gamma_1^3 + \gamma_1^2\xi + 4\gamma_1\Delta_{so}^2 - 2\xi\Delta_{so}^2) \\ &\quad + 2v^4k^4(\gamma_1 + \xi) \\ &\quad - \gamma_1(\gamma_1^4 + \gamma_1^3\xi + 2\gamma_1^2\Delta_{so}^2 + 2\gamma_1\xi\Delta_{so}^2 + 2\Delta_{so}^4), \end{aligned} \quad (31)$$

where $\xi = \sqrt{4v^2k^2 + \gamma_1^2}$. Thus, the conductivity may be written in the form

$$\sigma_{xy}^{s_z} = -\frac{e}{4\pi} \sum_n \int k R_n f(E_n) dk. \quad (32)$$

Taking into account the integrals

$$\int k R_1 dk = -\frac{\sqrt{2}(\gamma_1 + \xi)\Delta_{so}}{\xi(2v^2k^2 + \gamma_1^2 - \gamma_1\xi + 2\Delta_{so}^2)^{1/2}}, \quad (33)$$

$$\int k R_3 dk = \frac{\sqrt{2}(\gamma_1 - \xi)\Delta_{so}}{\xi(2v^2k^2 + \gamma_1^2 + \gamma_1\xi + 2\Delta_{so}^2)^{1/2}}, \quad (34)$$

and then assuming the appropriate limits of the integration, one finds the final expressions for the spin Hall conductivity as presented below.

When the chemical level is inside the gap, $|\mu| < \Delta_{so}$, the spin Hall conductivity is equal to

$$\sigma_{xy}^{s_z} = -2\frac{e}{4\pi}. \quad (35)$$

When $\Delta_{so} < |\mu| < \sqrt{\gamma_1^2 + \Delta_{so}^2}$,

$$\sigma_{xy}^{s_z} = -\frac{2(\gamma_1 + \sqrt{\mu^2 - \Delta_{so}^2})}{2\sqrt{\mu^2 - \Delta_{so}^2} + \gamma_1} \frac{\Delta_{so}}{|\mu|} \frac{e}{4\pi}, \quad (36)$$

while for $|\mu| > \sqrt{\gamma_1^2 + \Delta_{so}^2}$ one finds

$$\sigma_{xy}^{s_z} = -\frac{2(\mu^2 - \Delta_{so}^2) - \gamma_1^2}{4(\mu^2 - \Delta_{so}^2) - \gamma_1^2} \frac{4\Delta_{so}}{|\mu|} \frac{e}{4\pi}. \quad (37)$$

The spin Hall conductivity inside the gap is now twice as large as that in the case of a single-layer graphene. The general behavior of the conductivity with position of the Fermi level, shown in Fig.3 by the solid dark (solid red) line, is qualitatively similar to that for a single-layer graphene, i.e., outside the gap the spin Hall conductivity tends to zero with increasing $|\mu|$, while it remains constant and quantized inside the gap. This behavior is reasonable as the spin Hall conductivity is due to spin-orbit coupling, which is the same for both atomic monolayers. Note, the formula derived correspond to one Dirac point, while the figures include contributions from both Dirac points.

The corresponding spin Nernst conductivity is given by the following formulas:

When $\Delta_{so} < |\mu| < \sqrt{\gamma_1^2 + \Delta_{so}^2}$,

$$\alpha_{xy}^{sz} = \pm \frac{\pi}{6} k_B^2 \frac{\Delta_{so}}{\mu^2} T \times \frac{-\gamma_1^2 - 2\mu^2 - \frac{4\gamma_1\mu^2}{\sqrt{\mu^2 - \Delta_{so}^2}} + \Delta_{so}^2 \left(2 + \frac{3\gamma_1}{\sqrt{\mu^2 - \Delta_{so}^2}}\right)}{4\gamma_1\sqrt{\mu^2 - \Delta_{so}^2} + 4\mu^2 + \gamma_1^2 - 4\Delta_{so}^2}. \quad (38)$$

For $|\mu| > \sqrt{\gamma_1^2 + \Delta_{so}^2}$,

$$\alpha_{xy}^{sz} = \mp \frac{\pi}{3} \Delta_{so} k_B^2 T \times \frac{8\Delta_{so}^4 + 6\Delta_{so}^2\gamma_1^2 + \gamma_1^4 - 2(8\Delta_{so}^2 + 5\gamma_1^2)\mu^2 + 8\mu^4}{\mu^2(4\Delta_{so}^2 + \gamma_1^2 - 4\mu^2)^2}. \quad (39)$$

In turn, when μ is in the gap, $|\mu| < \Delta_{so}$, the spin Nernst conductivity vanishes, $\alpha_{xy}^{sz} = 0$. The signs $-$ and $+$ in the above formulas correspond to the case when the chemical potential is negative or positive, respectively.

Variation of the spin Nernst conductivity with the chemical level is shown in Fig. 3 by the solid gray (solid blue) line. Similarly as in a single-layer graphene¹⁸, the spin Nernst conductivity vanishes for the Fermi level inside the gap, when the system is in the insulating phase, and becomes nonzero for the Fermi level inside the valence or conduction bands, when the temperature gradient generates a longitudinal charge current. Note, the spin Nernst conductivity becomes divergent as μ approaches edges of the energy gap.

Conductivity in the tight binding model can be obtained in a similar way, although the corresponding formulas are cumbersome and will not be presented here. Instead of this we present some numerical results, which in Fig.3 are shown by the dotted lines. Note, the spin Hall as well as spin Nernst conductivities in the effective model coincide very well with the results obtained from the tight binding model.

B. The case of $V \neq 0$

Let us consider now the case of $V \neq 0$. The procedure presented above for the effective model with $V = 0$ can

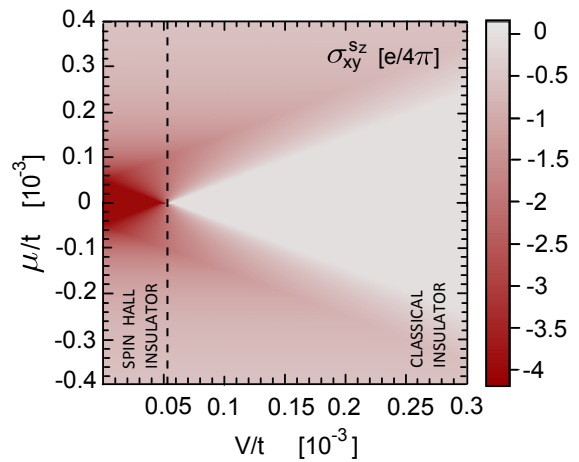


FIG. 4. (color on-line) Zero-temperature spin Hall conductivity as a function of the vertical voltage V and position of the Fermi level for the effective model described by the parameters given in Fig.2. Contributions from both Dirac points are included. The vertical dashed line corresponds to V , where transition from the spin Hall insulator to conventional insulator takes place.

be easily extended to a nonzero vertical bias, $V \neq 0$. The difference is that now the degeneracy of the bands is lifted and we have 8 different bands, $n = 1 - 8$, which have to be taken into account. Thus, instead of Eq.(27) we have now

$$\mathcal{F}(\varepsilon) = \frac{\chi(\varepsilon)}{\prod_{n=1}^8 [\varepsilon - E_n + \mu + i\delta \text{sign}(\varepsilon)]^2} \quad (40)$$

with adequate $\chi(\varepsilon)$. Following the procedure described above for $V = 0$, one can derive the corresponding analytical formula. These formula, however, will not be presented here as they are rather cumbersome, so we present only numerical results. Moreover, since the results in the tight binding model coincide with those obtained with the effective Hamiltonian, as shown above, we restrict the analysis below to the effective Hamiltonian.

In Fig.4 we show the spin Hall conductivity as a function of the Fermi level μ and vertical bias V . For $V = 0$ we recover the quantized conductivity in the gap. As V increases, however, the range of quantized spin Hall conductivity shrinks and at a certain value of V (indicated by the dashed line in Fig.4) there is a transition (at $\mu = 0$) from $\sigma_{xy}^{sz} = -4(e/4\pi)$ to $\sigma_{xy}^{sz} = 0$. This behavior is explicitly shown in Fig.5, where several cross-sections of Fig.4 along constant values of μ are presented. The above transition is clearly evident for the curve corresponding to $\mu = 0$.

The transition from topological insulating phase at small voltages to the normal insulating behavior at large voltages is also clearly visible in Fig.6, which presents some cross-sections of Fig.4 along constant values of V . This figure shows how the range of the quantized value of σ_{xy}^{sz} changes with increasing V . As V increases starting from $V = 0$, width of the range where σ_{xy}^{sz} is quantized

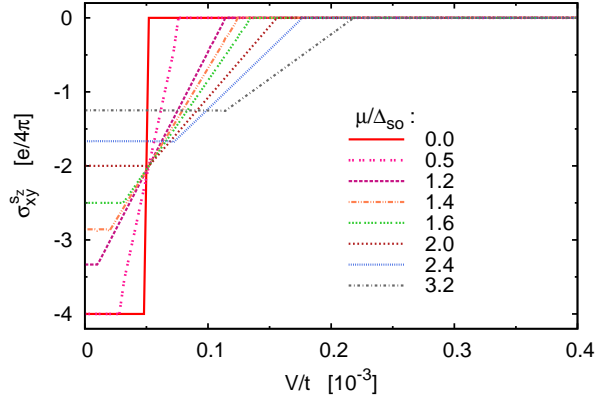


FIG. 5. (color on-line) Zero-temperature spin Hall conductivity as a function of vertical bias voltage V for indicated values of the Fermi energy. The curves correspond to crosssections of Fig.4 along constant μ . The other parameters as in Fig.4.

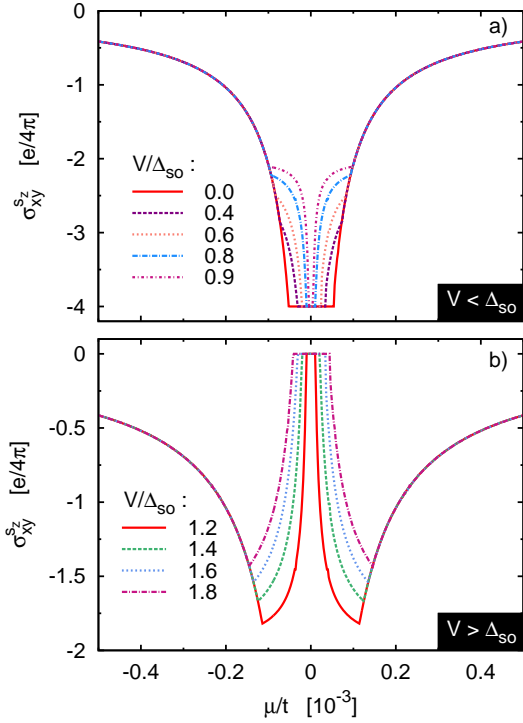


FIG. 6. (color on-line) Zero-temperature spin Hall conductivity as a function of the Fermi level for indicated values of the vertical bias voltage V . The curves correspond to crosssections of Fig.4 along constant V . The other parameters as in Fig.4.

shrinks, and at a certain critical value of V width of this range goes to zero. The spin Hall conductivity σ_{xy}^{sz} at $\mu = 0$ changes then from $\sigma_{xy}^{sz} = -4(e/4\pi)$ at voltages smaller than the critical one to $\sigma_{xy}^{sz} = 0$ at higher voltages. This clearly reveals a transition from the topological insulating phase to the normal insulating behavior (more information on the topological insulating phases in graphene can be found e.g. in Ref. [32]). From Figs 4 to 6 one could conclude that the gap diminishes with

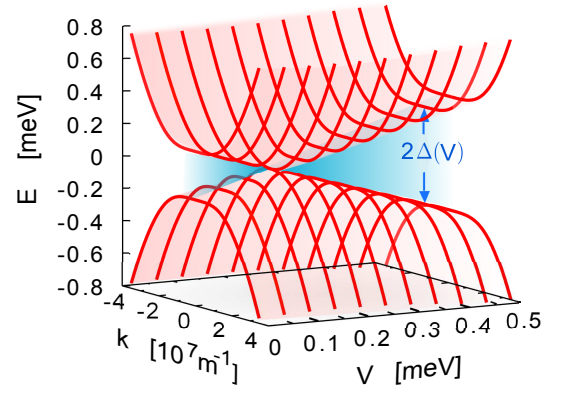


FIG. 7. (color on-line) Electronic spectra of the bilayer graphene in the vicinity of the Dirac point for different values of V . The curves show variation of the gap with increasing V , and closure of the gap at some critical value of V . The other parameters as in Fig.4

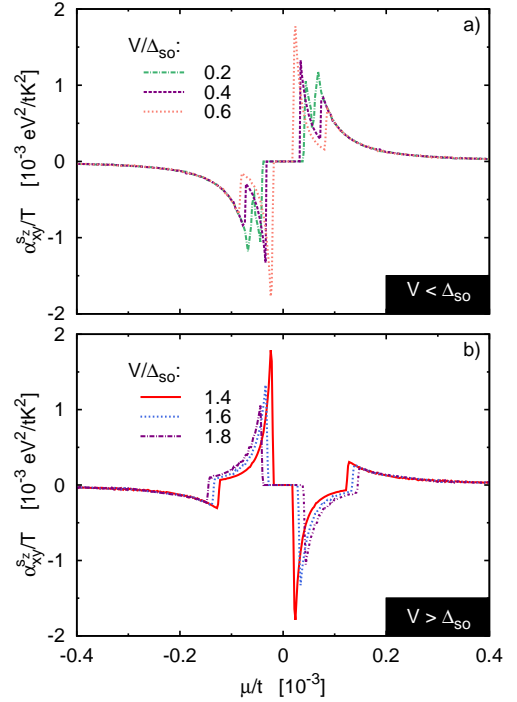


FIG. 8. (color on-line) Low-temperature spin Nernst conductivity as a function of the Fermi level for indicated values of V , calculated for the same parameters as in Fig.6.

increasing V , becomes totally suppressed at the critical value of V , and then becomes open again at larger voltages. Indeed, this is the case as shown in Fig.7, where the spectrum near the gap is plotted for several values of V . This figure clearly shows that the gap becomes closed at the critical value of V , and then is open again at larger values of V . The spin Hall conductivity in the gap above the critical voltage is however suppressed.

The phase transition from the topological spin Hall insulating phase to the conventional insulator becomes

revealed in the spin Nernst conductivity, too. This is presented in Fig.8, where the low-temperature spin Nernst conductivity is shown as a function of the Fermi energy for the same values of V as in Fig.6. The range of zero spin Nernst conductivity decreases with increasing V , goes to zero at the critical value of V , and then becomes nonzero again for larger values of V .

IV. LOW-ENERGY EFFECTIVE HAMILTONIAN

As we have already mentioned above, separation of the bands E_3 and E_4 (or $E_{3,3'}$ and $E_{4,4'}$) is much larger than separation of the bands E_1 and E_2 (or $E_{1,1'}$ and $E_{2,2'}$). The latter determines the energy gap induced by the spin-orbit coupling (see Fig.2). When only the electron states near the Fermi level are relevant and the Fermi level is in the gap or close to it, one may further reduce the effective Hamiltonian to include explicitly the bands $E_{1,1'}$ and $E_{2,2'}$, and the other bands only via effective parameters of the corresponding reduced effective model. The relevant reduced low-energy effective Hamiltonian takes the form²⁸:

$$H_K^r = \begin{bmatrix} \Delta_{so} + V & 0 & -\frac{\hbar^2 k_-^2}{2m} & 0 \\ 0 & -\Delta_{so} + V & 0 & -\frac{\hbar^2 k_-^2}{2m} \\ -\frac{\hbar^2 k_+^2}{2m} & 0 & -\Delta_{so} - V & 0 \\ 0 & -\frac{\hbar^2 k_+^2}{2m} & 0 & \Delta_{so} - V \end{bmatrix} \quad (41)$$

where $k_{\pm} = k_x \pm ik_y$ and $m = \gamma_1/2v_F$ is the effective electron mass. In the following we consider some special cases.

A. The case of $V = 0$

The corresponding eigenvalues of the Hamiltonian (41) are then equal to

$$E_{1,2} = \mp \left[\Delta_{so}^2 + \left(\frac{\hbar^2 k^2}{2m} \right)^2 \right]^{1/2}, \quad (42)$$

see the inset in Fig.9. Using the notation introduced in the preceding section we find

$$\sigma_{xy}^{sz} = i \frac{e}{2} \int \frac{d\varepsilon}{2\pi} \int \frac{d^2\mathbf{k}}{(2\pi)^2} \frac{\chi(\varepsilon)}{\prod_{n=1}^{n=2} [\varepsilon - E_n + \mu + i\delta \text{sgn}(\varepsilon)]^4}, \quad (43)$$

where

$$\chi(\varepsilon) = \frac{4\Delta_{so}\hbar^4 k^2}{m^2} \left[\Delta_{so}^2 - (\varepsilon + \mu)^2 + \left(\frac{\hbar^2 k^2}{2m} \right)^2 \right]^2 \quad (44)$$

Performing the integration over ε and then over \mathbf{k} , one arrives at the following analytical formulas for the spin

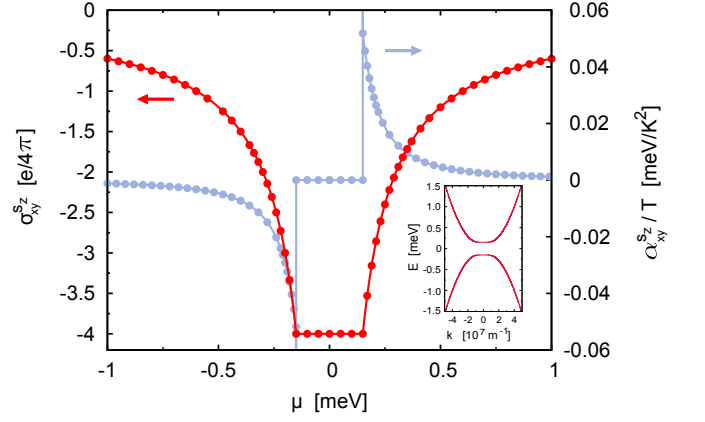


FIG. 9. (color on-line) Spin Hall and spin Nernst conductivities of a bilayer graphene for the low energy reduced Hamiltonian with the parameters corresponding to those assumed in Fig.2. Contributions from both K and K' points are included. The solid lines correspond to the results obtained from the Hamiltonian (10), while the dotted ones from the reduced Hamiltonian (41). The inset shows the energy spectrum corresponding to Eq.(42).

Hall conductivity:

$$\sigma_{xy}^{sz} = -\frac{2\Delta_{so}}{|\mu|} \frac{e}{4\pi} \quad (45)$$

for $|\mu| > \Delta_{so}$, and

$$\sigma_{xy}^{sz} = -2 \frac{e}{4\pi} \quad (46)$$

when the chemical level is inside the gap, $|\mu| < \Delta_{so}$.

The corresponding low-temperature spin Nernst conductivity is then given as follows. For $|\mu| > \Delta_{so}$ one finds

$$\alpha_{xy}^{sz} = \mp \frac{\pi}{6} k_B^2 \frac{\Delta_{so}}{\mu^2} T, \quad (47)$$

while for μ inside the gap $\alpha_{xy}^{sz} = 0$

The above results for both spin Hall and spin Nernst conductivities are shown by the dotted lines in Fig.9, where they are compared with the corresponding results obtained from the effective Hamiltonian (10) (solid lines). There is a nice agreement between the results. We note that the divergency of the spin Nernst conductivity when the Fermi level approaches the band edges, observed in the tight-binding and effective Hamiltonian, is not reproduced by the reduced Hamiltonian.

B. The case of $V \neq 0$

When $V \neq 0$ the eigenvalues of the Hamiltonian (41) take the form,

$$E_{1,2} = \mp \left[(V + \Delta_{so})^2 + \left(\frac{\hbar^2 k^2}{2m} \right)^2 \right]^{1/2}, \quad (48)$$

$$E_{1',2'} = \mp \left[(V - \Delta_{so})^2 + \left(\frac{\hbar^2 k^2}{2m} \right)^2 \right]^{1/2}. \quad (49)$$

The nonzero V leads to splitting of the electron bands, as already discussed above.

When $|\mu| > (V + \Delta_{so})$, the spin Hall conductivity is then given by

$$\sigma_{xy}^{sz} = -\frac{e}{4\pi} \frac{2\Delta_{so}}{|\mu|} \quad (50)$$

When $|V - \Delta_{so}| < |\mu| < (V + \Delta_{so})$,

$$\sigma_{xy}^{sz} = -\frac{e}{4\pi} \left(1 - \frac{V - \Delta_{so}}{|\mu|} \right) \quad (51)$$

Finally, when μ is inside the gap,

$$\sigma_{xy}^{sz} = 0 \quad \text{for } V > \Delta_{so} \quad (52)$$

$$\sigma_{xy}^{sz} = -2\frac{e}{4\pi} \quad \text{for } V < \Delta_{so}. \quad (53)$$

The corresponding low-temperature spin Nernst conductivity is given by

$$\alpha_{xy}^{sz} = \frac{\pi}{6} k_B^2 T \frac{\Delta_{so}}{|\mu|} \quad (54)$$

for $|\mu| > V + \Delta_{so}$, and

$$\alpha_{xy}^{sz} = -\frac{\pi}{12} k_B^2 T \frac{1}{|\mu|} (V - \Delta_{so}) \quad (55)$$

for $|V - \Delta_{so}| < |\mu| < (V + \Delta_{so})$. In turn, the spin Nernst conductivity vanishes inside the energy gap.

Behavior of spin Hall and spin Nernst conductivities with position of the Fermi level and bias voltage V almost coincides with that presented in Figs 4 to 6 and 8, and therefore will not be present here. As in the $\mathbf{k} \cdot \mathbf{p}$ model, one observes the same transition between the spin Hall insulator and classical insulator as V increases. As already mentioned above, there is no divergency of the spin Nernst conductivity at the band edge for the low energy effective model considered here.

V. SUMMARY

We have calculated analytically as well as numerically the spin Hall and spin Nernst conductivities in a bilayer graphene. To describe the relevant electronic spectrum we have assumed the tight binding model as well as some simplified effective Hamiltonians relevant for states close to the Dirac points. Both spin Hall and spin Nernst effects consist in transverse spin accumulation (spin current). However, as the spin Hall effect is due to external electric field, the Nernst effect is due to a temperature gradient. Assuming intrinsic spin orbit interaction, we have found the intrinsic contributions to both effects. Generally, the spin Hall conductivity in the energy gap of a bilayer graphene is twice as large as that for a single-layer graphene. When external voltage is applied between the two atomic sheets, we found a transition from the spin Hall insulator phase to the conventional insulator behavior. The energy gap at the transition point is closed.

We have compared results obtained from the tight-binding model with those derived from the effective Hamiltonians. From this comparison we arrived at the conclusion, that both spin Hall and spin Nernst conductivities are well described by the effective Hamiltonians, which allow derivation of some analytical results.

Acknowledgment

This work has been supported in part by the European Union under European Social Fund 'Human - best investment' (PO KL 4.1.1) and in part by funds of the Ministry of Science and Higher Education as a research project in years 2010-2013 (No. N N202 199239). The authors acknowledge valuable discussions with V.K. Dugaev.

¹ M. I. Dyakonov, V. I. Perel, Pis'ma Z. Eksp. Teor. Fiz. **13**, 657 (1971); JETP Lett. **13**, 467 (1971).

² M. I. Dyakonov, V. I. Perel, Phys. Lett. A **35**, 459 (1971).

³ J. E. Hirsch, Phys. Rev. Lett. **83**, 1834 (1999).

⁴ S. Murakami, N. Nagaosa, S. C. Zhang, Science **301**, 1348 (2003).

⁵ J. Sinova, D. Culcer, Q. Niu, N. A. Synitsyn, T. Jungwirth, A. H. MacDonald, Phys. Rev. Lett. **92**, 126603 (2004).

⁶ Y. K. Kato, R. C. Myers, A. C. Gossard, D. D. Awschalom, Science **306**, 1910 (2004).

⁷ T. Kimura, Y. Otani, Phys. Rev. Lett. **99**, 196604 (2007).

⁸ C. Brune, A. Roth, E. G. Novik, M. Konig, H. Buhmann, E. M. Hankiewicz, W. Hanke, J. Sinova, L. W. Molenkamp,

arXiv:0812.3768 (2008)

⁹ H. A. Engel, E. I. Rashba, B. I. Halperin, in *Handbook of Magnetism and Advanced Magnetic Materials*, edited by H. Kronmuller, S. Parkin, vol. 5: *Spintronics and Magneto-electronics*, John Wiley, New York, 2007.

¹⁰ S. A. Wolf, D. D. Awschalom, R. A. Buhrman, J. M. Daughton, S. von Molnár, M. L. Roukes, A. Y. Chtchelkanova and D. M. Treger, Science **294**, 1488 (2001)

¹¹ I. Zutíć, J. Fabian, S. Das Sarma, Rev. Mod. Phys. **76**, 323 (2004).

¹² V. Sih, D. D. Awschalom, J. Appl. Phys. **101**, 081710 (2007).

¹³ D. D. Awschalom, N. Samarth, Physics **2**, 50 (2009).

- ¹⁴ M. V. Berry, Proc. R. Soc. London, Ser. A **392**, 45 (1984).
- ¹⁵ G. Sundaram, Q. Niu, Phys. Rev. B **59**, 14915 (1999).
- ¹⁶ K. Uchida, S. Takahashi, K. Harii, J. Ieda, W. Koshihara, K. Ando, S. Meakawa, E. Saitoh, Nature **455**, 778 (2008).
- ¹⁷ D. Xiao, Y. Yao, Z. Fang, Q. Niu, Phys. Rev. Lett. **97**, 026603 (2006).
- ¹⁸ C. Zhang, S. Tewari and S. Das Sarma, Phys. Rev. B **79**, 245424 (2009).
- ¹⁹ C. M. Jaworski, J. Yang, S. Mack, D. D. Awschalom, J. P. Heremans, R. C. Myers, Nature Materials **9**, 898 (2010).
- ²⁰ A. K. Geim and K. S. Novoselov, Nature Mater. **6**, 183 (2007).
- ²¹ M. I. Katsnelson, Mater. Today **10**, 20 (2007).
- ²² A. H. Castro Neto, F. Guinea, N. M. R. Peres, K. S. Novoselov and A. K. Geim, Rev. Mod. Phys. **81**, 109 (2009).
- ²³ C. L. Kane and E. J. Mele, Phys. Rev. Lett. **95**, 226801 (2005).
- ²⁴ F. Guinea, New Journal of Physics **12**, 083063 (2010).
- ²⁵ E. V. Castro, K. S. Novoselov, S. V. Morozov, N. M. R. Peres, J. M. B. Lopes dos Santos, J. Nilsson, Phys. Rev. Lett. **99**, 216802 (2007).
- ²⁶ Y. Zhang, Tsung-Ta Tang, C. Girit, Z. Hao, M. C. Martin, A. Zettl, M. F. Crommie, Y. R. Shen, F. Wang, Nature **459**, 820 (2009).
- ²⁷ E. Prada, P. San-Jose, L. Brey, H. A. Fertig, Solid State Comm. **151**, 1075 (2011).
- ²⁸ E. McCann, D. S. L. Abergel, V. I. Fal'ko, Solid State Communications **143**, 110 (2007).
- ²⁹ A. Dyrdał, V. Dugaev, J. Barnaś, Phys. Rev. B **80**, 155444 (2009).
- ³⁰ D. Xiao, J. Shi, Q. Niu, Phys. Rev. Lett. **95**, 137204 (2005).
- ³¹ C.-P. Chuu, M.-C. Chang, Q. Niu, Solid State Communications **150**, 533 (2010).
- ³² A. Cortijo, A. G. Grushin, M. A. H. Vozmediano, Phys. Rev. B **82**, 195438 (2010).